Emergent nontrivial lattices for topological insulators

O. Dutta,[1,2,*] A. Przysiężna,[3,4] and M. Lewenstein[1,5]

[1]*Institut de Ciencies Fotoniques (ICFO), Avenida Carl Friedrich Gauss 3, 08860 Castelldefels (Barcelona), Spain*
[2]*Instytut Fizyki imienia Mariana Smoluchowskiego, Uniwersytet Jagielloński, ulica Reymonta 4, PL-30-059 Kraków, Poland*
[3]*Institute of Theoretical Physics and Astrophysics, University of Gdańsk, Wita Stwosza 57, 80-952 Gdańsk, Poland*
[4]*National Quantum Information Centre of Gdańsk, Andersa 27, 81-824 Sopot, Poland*
[5]*Institucio Catalana de Recerca i Estudis Avançats (ICREA), Lluis Companys 23, E-08010 Barcelona, Spain*

(Received 12 June 2013; published 3 April 2014)

Materials with nontrivial lattice geometries allow for the creation of exotic states of matter like topologically insulating states. Therefore searching for such materials is an important aspect of current research in solid-state physics. In the field of ultracold gases there are ongoing studies aiming to create nontrivial lattices using optical means. In this paper we study two species of fermions trapped in a square optical lattice and show how nontrivial lattices can emerge due to strong interaction between atoms. We theoretically investigate regimes of tunable parameters in which such self-assembly may take place and describe the necessary experimental conditions. Moreover, we discuss the possibility of such emergent lattices hosting topologically insulating states.

DOI: 10.1103/PhysRevA.89.043602 PACS number(s): 67.85.Lm, 03.75.Lm, 73.43.−f

I. INTRODUCTION

Complex systems are characterized by a large number of locally interacting elements with properties that cannot be derived as a sum of local individual elements [1]. In such systems spontaneous self-assembly [2] takes place and *emergent* structures are formed from disorder due to the cooperative effect of the interacting system. Such emergent behavior of complex systems is responsible for many organized structures found in many-body physics, chemistry, biological systems, etc. In the present paper we show that cooperation of interaction and orbital effects in a lattice can result in nontrivial emergent structures (lattices) with topological order.

Nontrivial lattice geometries are at the heart of various exotic phenomena in many-body physics. One promising playground for the realization of such exotic lattices and states is ultracold gases trapped in lattice potentials [3]. This is due to the high degree of experimental controllability and tunability that ultracold systems exhibit. In this field, a variety of nontrivial lattice geometries was experimentally created by using counter-propagating laser beams in different configurations [4–7]. These lattices can be than used to realize exotic states by introducing tunable long-range hopping amplitudes [8–12]. Particularly interesting is the possibility of creating topologically insulating states [13–15] that allow for a robust transport of charges (matter) on the boundary and thus have potential applications in spintronics, quantum computing [16], and spintomics [3].

In this paper we propose an alternative route to the creation of nontrivial lattice geometries. Our system consists of strongly attractive two-species fermions trapped in a square optical lattice. We show that the strong interaction and orbital effects can give rise to the emergence of nontrivial lattice structures and pseudospin degrees of freedom by self-assembly of an ultracold gas. The emerging lattice is characterized by topologically protected band crossing points. This effect is counterintuitive, as strong attraction in general destroys topological order. As an example of topological properties, we discuss the appearance of interaction-driven topological insulating states: the quantum anomalous Hall (QAH) state, characterized by a spontaneously broken time-reversal symmetry with a gap in the bulk and quantized Hall conductivity; and the quantum spin Hall (QSH) state, which can be identified as two copies of QAH states, which, on the whole, preserves the time-reversal symmetry.

Our proposal shows that nontrivial topological properties are induced by the interplay between strong interactions and orbital effects. One feature of the present proposal is that our system can contain self-generated impurities, domain structures, etc., due to the spontaneous nature of our emergent lattice. The presence of such imperfections is crucial to observe phenomena such as edge currents and Hall plateaus. This is in contrast to optically created frustrated lattices, where one has to impose additional nontrivial potential to create such imperfections.

II. MODEL

We consider a mixture of two-species ultracold fermionic atoms trapped in an optical lattice potential $V_{\sigma,\mathrm{latt}} = V_{\sigma,x}\sin^2(\pi x/a) + V_{\sigma,y}\sin^2(\pi y/a) + V_{\sigma,z}\sin^2(\pi z/a)$, where $\sigma = \uparrow$ and $\sigma = \downarrow$ denote the species and $V_{\sigma,x(y)(z)}$ are the corresponding lattice depths for σ-fermions along the x, y, and z directions, respectively. The lattice constant a is given by the trapping laser wavelength, $a = \lambda/2$. For the two-dimensional (2D) geometry we choose $V_0 = V_{\downarrow,x} = V_{\downarrow,y}$, $V_1 = V_{\downarrow,z} = V_{\uparrow,x(y)(z)}$, and $V_1 \gg V_0$, so that the $\downarrow$-fermions can effectively move in the x-y plane with the z motion frozen. Since the $\uparrow$-fermions move in a deeper lattice, in the first approximation we can neglect the tunneling of these particles. For simplicity, we consider the case in which fermionic masses are equal, $m_\downarrow = m_\uparrow$, which implies equal recoil energies $E_R = E_{R\sigma} = \pi^2\hbar^2/2m_\sigma a^2$. In this paper we look into a spin-imbalanced situation with fillings $n_\downarrow = 1$ and $n_\uparrow = 1/2$. It is worth mentioning that such attractive fermion mixtures have already been realized in optical lattices for studying superfluidity [17], anomalous transport [18,19], etc.

*omjyoti@gmail.com

Atoms of different types interact with each other via s-wave scattering with strength a_s. If the interaction is strongly attractive ($a_s \ll 0$), the $\uparrow$- and $\downarrow$-fermions tend to pair and form composites with creation operator $\hat{b}^\dagger_{\mathbf{i}} = \hat{s}^\dagger_{\uparrow\mathbf{i}}\hat{s}^\dagger_{\downarrow\mathbf{i}}$ and corresponding number operator $\hat{n}^B_{\mathbf{i}}$ [20–22]. Here $\hat{s}^\dagger_{\sigma\mathbf{i}}$ and $\hat{s}_{\sigma\mathbf{i}}$ are the creation and annihilation operators of the σ-fermions in the respective s bands. The composite density is the same as the $\uparrow$-fermion density, i.e., in our case, $n_\uparrow = n^B = 1/2$. Such composites are considered static due to the smallness of the tunneling of the minority component. The excess $\downarrow$-fermions with filling $m = n_\downarrow - n_\uparrow = 1/2$ can tunnel from one site to another. Recently it has been noted that in the strong-interaction regime, the standard Hubbard models have to be modified due to both intra- and interband effects [23–26]. Taking these effects into account we construct a minimal model for the composites and the excess $\downarrow$-fermions by including the occupation of the s and p bands and the renormalization of the interactions.

III. MODIFIED HAMILTONIAN

The inclusion of the p bands allows one $\downarrow$-fermion to occupy the same site as a composite. The single-particle tunneling Hamiltonian then reads

$$H_{\mathrm{t}} = -J_0 \sum_{\langle \mathbf{ij}\rangle} \hat{s}^\dagger_{\mathbf{i}}\hat{s}_{\mathbf{j}} + J_1 \sum_{\delta}\sum_{\langle \mathbf{ij}\rangle_\delta} \hat{p}^\dagger_{\delta\mathbf{i}}\hat{p}_{\delta\mathbf{j}}, \tag{1}$$

where $\delta = x, y$ and $\hat{s}^\dagger_{\mathbf{i}}, \hat{s}_{\mathbf{i}}$, $\hat{p}^\dagger_{\delta\mathbf{i}}, \hat{p}_{\delta\mathbf{i}}$ are the creation and annihilation operators of the $\downarrow$-fermions in the s and p bands, respectively. $J_0, J_1 > 0$ are the single-particle tunneling amplitudes in the s and p bands respectively, and $\langle \mathbf{ij}\rangle_{x(y)}$ denotes the nearest-neighbor sites along the $x(y)$ direction.

The on-site Hamiltonian for the excess $\downarrow$-fermions and the composites including the s and p bands is given by

$$\begin{aligned} H_{\mathrm{int}} = &-|U_2| \sum_{\mathbf{i}} \hat{n}^B_i(1-\hat{n}_{x\mathbf{i}})(1-\hat{n}_{y\mathbf{i}}) \\ &- |U_3| \sum_{\mathbf{i}} \hat{n}^B_{\mathbf{i}}(\hat{n}_{x\mathbf{i}} + \hat{n}_{y\mathbf{i}}) - |\delta U_3| \sum_{\mathbf{i}} \hat{n}_{x\mathbf{i}}\hat{n}_{y\mathbf{i}}\hat{n}^B_{\mathbf{i}} \\ &+ E_1 \sum_{\mathbf{i}} (\hat{n}_{x\mathbf{i}} + \hat{n}_{y\mathbf{i}}), \end{aligned} \tag{2}$$

where $\hat{n}_{x(y)\mathbf{i}} = \hat{p}^\dagger_{x(y)\mathbf{i}}\hat{p}_{x(y)\mathbf{i}}$. The renormalized self-energy of the composite is given by U_2, whereas U_3 is the strength of the renormalized on-site interactions between a composite and a $\downarrow$-fermion in the p_x (p_y) orbital at a given site. δU_3 denotes the effective three-body interaction between one composite and two $\downarrow$-fermions each in the p_x and p_y orbitals. The origin of the effective three-body interaction comes from the excitations to higher bands. Such higher-body interactions like δU_3 have been probed in ultracold atom experiments [27] and are different from the few-body phenomena like three-body bound states arising in Efimov physics [28]. We find that δU_3 is small compared to other parameters, so we neglect it at first. Then the energy cost for an excess $\downarrow$-fermion to occupy the p band of a composite occupied site is given by

$$\Delta = E_1 + (U_3 - U_2) \tag{3}$$

and can be reduced as one increases the attractive scattering length. When Δ is small or negative, the $\downarrow$-fermions can occupy the p orbital of a site with a composite.

Next we consider two modifications originating from the nearest-neighbor scattering due to the interaction between the excess $\downarrow$-fermions and the composites. The first of the modifications mixes the s and p bands and can be written as

$$H_{01} = J_{01} \sum_{\delta=x,y}\sum_{\langle \mathbf{ij}\rangle_\delta} \zeta_{i_\delta, j_\delta} \hat{p}^\dagger_{\delta\mathbf{i}}\hat{n}^B_{\mathbf{i}}\hat{s}_{\mathbf{j}} + \mathrm{H.c.}, \tag{4}$$

where J_{01} denotes the interaction-induced interband tunneling and $\zeta_{i_\delta, j_\delta} = (-1)^{i_\delta - j_\delta}$ reflects the staggered nature of the s-p tunneling matrix. This process is shown in Fig. 1(b), where a $\downarrow$-fermion in the s orbital is scattered to the p orbital of the neigboring site due to the interaction with a composite. Such natural nonlocal hybridization between$s$-p bands due to interaction-induced tunneling is an important feature of the strongly interacting gases in lattices. It is worth stressing that such processes are usually neglected in the literature. Another feature of such s-p hybridization is that, due to parity, any tunneling processes like $\hat{p}^\dagger_{y\mathbf{i}}\hat{n}^B_{\mathbf{i}}\hat{s}_{\mathbf{j}}$ vanishes for $\mathbf{i} = (i_x, i_y)$ and $\mathbf{j} = (i_x \pm 1, i_y)$.

The second modification describes the interaction-induced tunneling in the p band, expressed as

$$H_{\mathrm{T}} = J_{11} \sum_{\delta}\sum_{\langle \mathbf{ij}\rangle_\delta} \hat{p}^\dagger_{\delta\mathbf{i}}\left(\hat{n}^B_{\mathbf{i}} + \hat{n}^B_{\mathbf{j}}\right)\hat{p}_{\delta\mathbf{j}}, \tag{5}$$

where J_{11} denotes intraband interaction-induced tunneling for p_x (p_y)-fermions along the x (y) direction. H_T gives the most

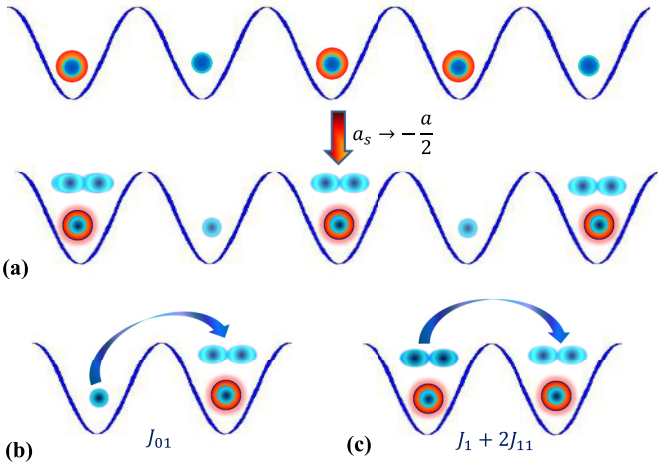

FIG. 1. (Color online) One-dimensional schematic representation of the system considered. A larger (red) sphere refers to a $\uparrow$-fermion and a smaller (blue) sphere represents a $\downarrow$-fermion. (a) Top: One creates a band insulator for $\downarrow$-fermions and a half-filled system for $\uparrow$-fermions in the presence of weak interactions. Bottom: Increasing the attractive scattering length a_s leads to the emergence of composites that form a checkerboard structure and the remaining $\downarrow$-fermions move between s and p orbitals (blue spheres and dumbbells). (b) The interaction-induced s-p band hybridization tunneling element corresponding to Hamiltonian (4). (c) Effective tunneling in the p band when two composites occupy neighboring sites.

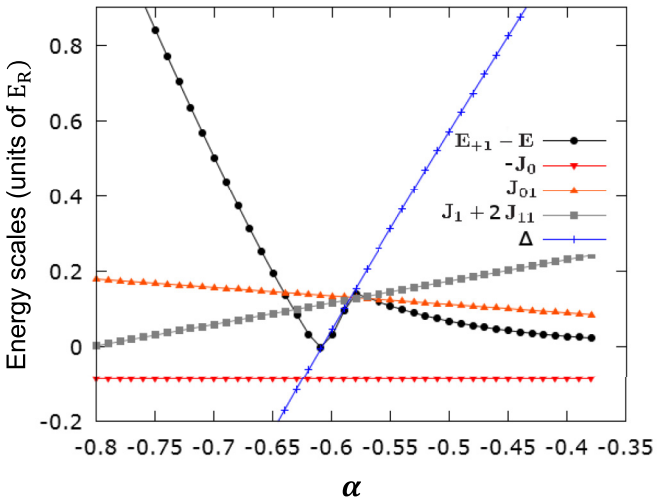

FIG. 2. (Color online) Comparison of different energy scales present in the system as a function of the effective interaction strength. Color lines represent different hopping parameters. The black line with circles represents the energy difference between the state of a system with half-filling of a ↑-fermion (**E**) and a state with one ↑-fermion more than half-filled ($\mathbf{E}_{+1}$). Energies are in units of E_R, and lattice depths are $V_0 = 4E_R$ and $V_1 = 20E_R$.

important contribution to the renormalization of intraband tunneling [26]. Tunneling in the p band is possible only when two neighboring sites are occupied by composites [see Fig. 1(c)], as this process conserves energy. For $a_s < 0$, the interaction-induced tunneling J_{11} is negative and the effective tunneling in the p band (given by $J_1 + 2J_{11}$) decreases with increasing attraction. Thus in the region where $|J_{01}| \sim |J_1 + 2J_{11}|$, the excess ↓-fermions prefer a configuration with alternating sites occupied by composites [Fig. 1(b)]. The relevant tunneling parameters and interaction parameters are controlled only by the effective interaction $\alpha = a_s/a$ and the lattice depths. Their derivation using Wannier functions is discussed in Appendixes A and B. The magnitudes of the various tunneling amplitudes and Δ are shown in Fig. 2.

It is worth noting here that the total Hamiltonian has features similar to those of the Falicov-Kimball (FK) model. The FK model describes interaction between localized classical modes and itinerant quantum modes of a system. It was first proposed to study metal-insulator transitions in mixed valence compounds of rare earth and transition metal oxides [29] and to study crystallization [30]. However there exists one important distinction between the FK model and our present study. Namely, FK models do not possess the correlated multiorbital tunneling processes. In the system that we investigate these processes not only are present but also play a crucial role.

IV. DYNAMICAL LIEB LATTICE

In this section, we discus the possible ground-state structures of our system characterized by the total Hamiltonian $H = H_t + H_T + H_{01} + H_{int}$. The total Hamiltonian H does not contain composite tunneling and the commutator $[\hat{n}_i^B, H] = 0$. Therefore $n_i^B = 0,1$ becomes a good quantum number. We find the ground state of the system by comparing the energies of different configurations of n_i^B over the entire lattice. The search space is too large to compare the energy of every single configuration. Therefore we locate a good approximation to the global optimum by using simulated annealing [31,32] (For details see Appendix C). We find the lowest energy configurations of the composites for various parameters on a 12×12 lattice with periodic boundary conditions. While calculating the energy for every single configuration, we take into account weak attraction between the orbitals [Eq. (2)] using the Hartree-Fock approximation. The resulting phase diagram for the composites is shown in Fig. 3(a). We distinguish the following phases for the composites: (i) a checkerboard structure with period 1 [CH1; Fig. 3(b)], (ii) a mixed phase characterized by the absence of any periodic structure, and (iii) a phase-separated state characterized by the clustering of the composites to one region of the lattice. The mixed phase occurs in the region where the energy cost to occupy the p orbital is low compared to that of other tunneling processes. Thus it is possible that the mixed phases contain self-generated disorder due to the composite density dependence on the tunneling processes. We have checked the existence of the mixed phases and obtained phase boundaries

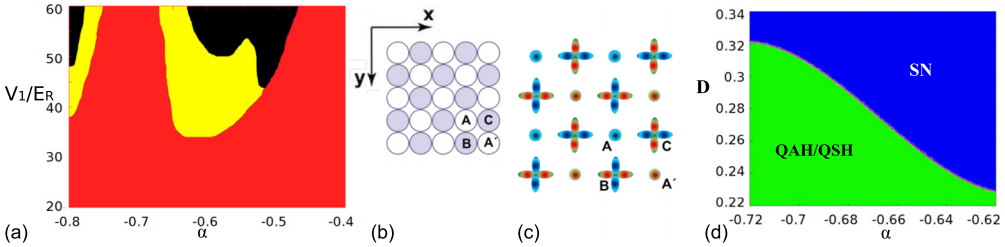

FIG. 3. (Color online) (a) Phase diagram for the configurations of the composites. The largest (red) region denotes the period 1 checkerboard (CH1) configuration for the composites. The black region denotes the phase-separated state; the yellow region, the mixed phase. The shallow lattice parameter is $V_0 = 4E_R$. (b) Distribution of the composites in the CH1 phase. Filled (open) circles denote the presence (absence) of a composite. (c) Orbital degree of freedom for the excess ↓-fermions in the *CH1* lattice. Colored circles denote s orbitals. Horizontal (vertical) dumbbell shapes denote $p_x(p_y)$ orbitals. Basis states for the blue (red) lattice are denoted **A**,**B**, and **C** (**A**′,**B**, and **C**). The corresponding sites in the CH1 structure are shown in Fig. 2(b). (d) Ground-state phase diagram for excess ↓-fermions corresponding to the composite CH1 phase. Phases are shown as a function of the dipolar strength D and contact interaction strength α for $V_0 = 4E_R$. The upper (blue) region denotes the spin-nematic (SN) phase, whereas the lower (green) region denotes quantum anomalous Hall and quantum spin Hall (QAH/QSH) phases.

also for lattice sizes of 8×8 and 16×16 and the phase boundaries remain qualitatively unchanged.

The CH1 region is the most interesting one with respect to the generation of nontrivial topological lattices. In the parameter regime, for lattice depth $V_1 \lesssim 35E_R$ with $V_0 = 4E_R$, we find that the CH1 region becomes the ground state. In the rest of this paper we concentrate on this particular parameter space. The presence of the CH1 region can be qualitatively predicted for $\Delta \ll 0$ and it can be easily shown that the CH1 structure has the lowest energy provided that $2J_{01}^2/|\Delta| > |J_1 + 2J_{11}|/\pi$. On the other hand, for $\Delta > 0$, the CH1 structure has the lowest energy as long as $J_{01}^2/|\Delta| \neq 0$.

We also note that the origin of the CH1 structure is different from the origin of the antiferromagnetic Neel phase for the repulsive Fermi-Hubbard model. For repulsive fermions, the Neel state arises in the balanced mixture due to the lowering of energy in the form of second-order exchange processes due to tunneling induced-localized creation of pairs. On the other hand, in the present case, the excess fermions are delocalized over the whole lattice. Then the CH1 structure appears as a result of the minimization of the total kinetic energy of the delocalized excess $\downarrow$-fermions. Moreover, we examine the energy cost related to the addition of the minority component. In Fig. 2, we plot the energy cost to dope the CH1 phase with an additional minority component for lattice depths $V_0 = 4E_R$ and $V_1 = 20E_R$. The energy cost is denoted $\mathbf{E_{+1}} - \mathbf{E}$. We see that in the regime of $\Delta < 0$ it costs additional energy of the order $\sim|\Delta|$ to dope with a minority component. In the regime of negative Δ, this energy cost, $\mathbf{E_{+1}} - \mathbf{E}$, is much larger than the other tunneling processes (Fig. 2). The CH1 phase is then robust against small doping of minority components.

Now, we focus our attention on the behavior of the excess mobile fermions. The excess fermions move on the CH1 structures created by the composites. Considering the distribution of the orbitals that excess fermions can occupy, the motion of these particles can be divided into two sublattices, shown in blue and red in Fig. 3(c). In order to see this, let us consider the empty site A, shown in the composite structure in Fig. 3(b). The s orbital at this site [shown as the blue site denoted A in Fig. 3(c)] can be occupied by an excess fermion. Then the fermion occupying site A can move to either the p_x orbital of the B site or the p_y orbital of the C site under the influence of Hamiltonian (4). This is due to the fact that both site B and site C are occupied by composites as denoted by dark circles in Fig. 3(a). Then due to the absence of any tunneling matrix element between the p_x orbital at site B (p_y orbital of site C) and the s orbital at site A$'$, the excess particles will only move in the blue sublattice as shown in Fig. 3(c). Similarly, one can construct the red sublattice geometry. This takes place because of the directional nature of the interorbital tunneling J_{01} in Hamiltonian (4) and the absence of any on-site orbital mixing term in (2) due to parity and fermionic statistics. Each of the sublattices in Fig. 3(c) can be characterized by three basis sites, denoted **A**, **B**, and **C** (for the blue lattice) and **A**$'$, **B**, and **C** (for the red lattice). Both the red and the blue sublattices have the structure of a Lieb lattice [33]. Let us denote the excess $\downarrow$-fermions moving in the blue sublattice $\Phi_1 = [\hat{s}_A, \hat{p}_{yB}, \hat{p}_{xC}]$ and those in the red sublattice $\Phi_2 = [\hat{s}_{A'}, \hat{p}_{xB}, \hat{p}_{yC}]$. We can see that, due to the interaction, we induce 1 pseudospin degree of freedom in the form of orbitals in different sublattices. Their motion is governed by the Hamiltonian

$$H = J_{01}\Bigg[\sum_{\langle \mathbf{ij}\rangle_x} \zeta_{i_x,j_x}\hat{s}^\dagger_{\mathbf{Ai}}\hat{p}_{\mathbf{xCj}} + \sum_{\langle \mathbf{ij}\rangle_y} \zeta_{i_y,j_y}\hat{s}^\dagger_{\mathbf{Ai}}\hat{p}_{\mathbf{yBj}} + \sum_{\langle \mathbf{ij}\rangle_x} \zeta_{i_x,j_x}\hat{s}^\dagger_{\mathbf{A'i}}\hat{p}_{\mathbf{xBj}} + \sum_{\langle \mathbf{ij}\rangle_y} \zeta_{i_y,j_y}\hat{s}^\dagger_{\mathbf{A'i}}\hat{p}_{\mathbf{yCj}} + \text{H.c.}\Bigg] + \Delta \sum_{\mathbf{i},\tau=\mathbf{B},\mathbf{C}} (\hat{n}_{\tau\mathbf{xi}} + \hat{n}_{\tau\mathbf{yi}}) - |\delta U_3| \sum_{\mathbf{i},\tau=B,C} \hat{n}_{x\tau\mathbf{i}}\hat{n}_{y\tau\mathbf{i}}. \quad (6)$$

Here the first term (inside the bracket) in Eq. (6) is a reformulation of H_{01} from Eq. (4). The second term refers to the energy cost of the p-orbital atoms occupying a site already taken by a composite. The third term describes effective on-site interactions between red and blue fermions at sites B and C. Now, let us focus on the single-particle dispersion relation. Diagonalizing the single-particle part of Hamiltonian (6), we get

$$\epsilon_{\mathbf{k}} \in \{\Delta, \Delta/2 \pm \sqrt{(\Delta/2)^2 + 4J_{01}^2[\sin^2 k_x a + \sin^2 k_y a]}\}, \quad (7)$$

where the momentum $\mathbf{k} = (k_x a, k_y a)$ belongs to the reduced Brillouin zone $(-\pi/2, \pi/2)$. The dispersion relation in Eq. (7) is plotted in Fig. 4 for three values of Δ. The dispersion contains a quadratic band crossing point (QBCP) for $\Delta \neq 0$

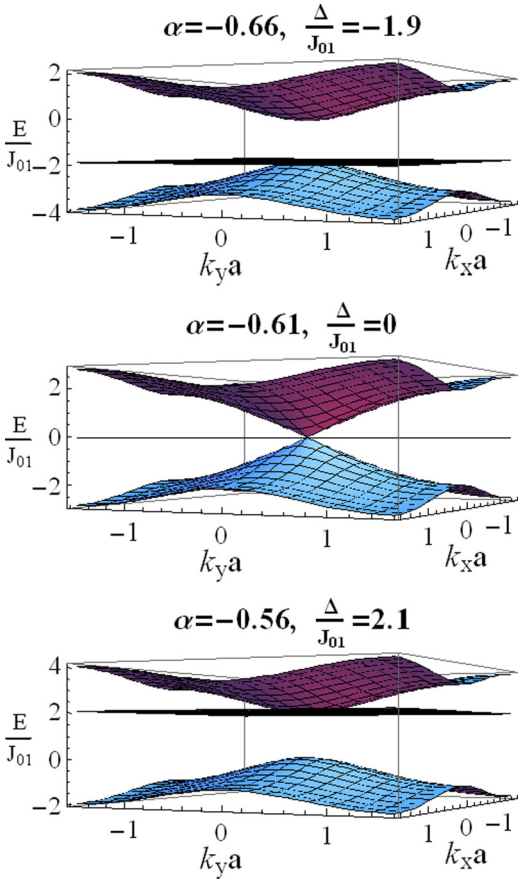

FIG. 4. (Color online) Dispersion relations of the Lieb lattice, as expressed in (7), for three values of Δ with lattice depths $V_0 = 4E_R$ and $V_1 = 20E_R$.

with one of the dispersive bands touching the flat band at momentum (0,0). For $\Delta = 0$, three bands touch each other at the momentum (0,0), with the upper and lower band having linear dispersions in the vicinity of this point. For simplicity let us consider only the case where $\Delta < 0$. We can write an effective two-band Hamiltonian $H = d_0\mathcal{I} + d_z\sigma_z + d_x\sigma_x$, where $\sigma_{x(z)}$ are the Pauli matrices, $\mathcal{I}$ is the identity matrix, $d_0 = -(J_{01}^2/\Delta)(\cos 2k_x a + \cos 2k_y a)$, and the vector $\vec{d} = (d_x, d_z) = -(J_{01}^2/\Delta)(4 \sin k_x a \sin k_y a, \cos 2k_x a - \cos 2k_y a)$. In this limit, the particles occupy only sites B and C of the lattice and the population at sites A and A′ is negligible. For excess fermion filling $m = 1/2$, the dispersive band is filled and any excitation to the next flat band remains localized in space. This makes the system an insulator. The next dispersive band is separated by an energy gap of Δ at $\mathbf{k} = (0,0)$. We introduce a normalized vector $\hat{d} = \vec{d}/\sqrt{|\vec{d}|}$ (mapping from the Brillouin zone to a two-sphere) and define the Berry phase as

$$B = \int d^2\mathbf{k}\, \hat{d} \cdot [\partial_{k_x}\hat{d} \times \partial_{k_y}\hat{d}], \tag{8}$$

with the integration over the Brillouin zone. The vector $\vec{d}$ acts like an effective magnetic field and the corresponding Berry phase is given by $\pm 2\pi$. The appearance of the nonzero Berry phase makes the QBCP topologically stable. Moreover, at excess fermion filling $m = 1/2$, the lower band is completely filled. The system remains insulating with the topological lower band filled. In this regard, the Lieb lattice is different from the honeycomb lattices, where near the band crossing points (Dirac points), there are linear dispersion relations. Because of the presence of the dispersive band at the crossing point, unlike the Dirac point, the system is unstable towards topologically insulating states even for the introduction of very small spin-orbit coupling.

We would like to point out that such emergent nontrivial lattice structures are not possible even if one realizes CH1 structures in different systems such as dipolar systems and atomic mixtures [34]. Even in the Falicov-Kimball model, due to the absence of such interorbital hybridization, a CH1 structure cannot give rise to a nontrivial lattice geometry for mobile fermions. Summarizing, in this section we have shown that, due to interaction-induced tunneling, one can generate topologically protected exotic lattices starting from trivial geometries.

V. PROPOSED EXPERIMENTAL REALIZATION

For experimental realization of the present proposal, we consider a band insulator for ↓-fermions and half-filling for ↑-fermions trapped on a square lattice where the interspecies interaction is weak. Such species-dependent lattices have been experimentally realized to study glassy behavior, as in Ref. [36]. Then by increasing the scattering length in the attractive regime via Feshbach resonance (or confinement-induced resonance), one can reach the regime of a dynamical Lieb lattice. As one gets to the region with $\Delta \approx 0$, the Lieb lattice emerges due to the CH1 structure of the composites. To experimentally detect this phase, one can probe the excitation spectrum of the mobile fermions using Bragg spectroscopy [37,38] or by using momentum-resolved intraband transitions [7]. Such measurements can show the signature of the Lieb lattice structure by showing the presence of a QBCP and the curvature of various bands. Additionally, measurement of the density-density correlations from the expansion of the minority component can give a signature for the CH1 structure [39] arrangement of the composites. The appearance of the CH1 structure over a wide range of lattice depths and scattering lengths, as shown in Fig. 3(a), indicates that this result is stable under small changes of parameters.

Next, we briefly discuss the role of tunneling of the minority ↑-fermions for experimental realization. The effective tunneling strength (denoted $J_\uparrow$) of the ↑-fermions includes both single-particle tunneling and contributions from the interaction. To reach the CH1 configuration, the tunneling of the ↑-fermions is important, as it helps to scan the large set of possible configurations for the composites. In the present situation [as depicted in Fig. 1(a)] for a relatively weak interaction ($\Delta > 0$), due to the high-density imbalance, almost every composite has an excess ↓-fermion as a nearest neighbor. Therefore, due to tunneling of the minority component, a composite can effectively move to a neighboring site that already contains excess ↓-fermions. Thus the time scale required to reach the CH1 lattice configuration is set by the minority component tunneling rate. Moreover, to generate long-range order over the entire system, one needs many such tunneling events. Subsequently the time scale to form the entire CH1 configuration will be set by the corresponding Lieb-Robinson bound. In that situation, within the time scale allowed by the loss rates, domains of CH1 order with different orientations will be created. For lattice depths $V_0 = 4E_R$ and $V_1 = 20E_R$ and interaction strength $a_s/a = -0.5$, we have found that the time scale for the CH1 pattern to occur is of the order of ∼1 ms. It is worth nothing that the situation here is different from the spin-balanced case. In the spin-balanced situation, the composites can only have a vacant neighbor where they can hop via a slow second-order process with strength $\sim J_0 J_\uparrow/|U_2|$, resulting in a slower redistribution of the pairs [18,35]. Due to the presence of hopping of the ↑-fermions, our calculations in the previous section are valid as long as $J_\uparrow \ll \{|J_{01}|, J_0, J_1 + 2J_{11}\}$. We have calculated that the various tunneling terms of the excess fermions (especially J_{01}) are at least one order of magnitude larger than $J_\uparrow$. Because of the separation of tunneling scales between the excess fermions and the composites, one can use a Born-Oppenheimer-like approximation and recover the FK-like Hamiltonian discussed in the present and previous sections.

Regarding the relevant atomic species for such experiments, one such choice could be a fermionic ^{6}Li species or fermionic ^{40}K. For a lattice constant of $a = 500$ nm, the corresponding scattering length is of the order of $a_s \sim -300$ nm. This has been achieved in lithium mixtures in Refs. [40–42] and in fermionic potassium mixtures in Ref. [43]. The other option is a mass-imbalanced mixture. In that case the effective scattering length is scaled and $\alpha \approx (a_s/a)(1 + m_\downarrow/2m_\uparrow)$ for the same parameters as used in the case of equal mass. Thus, if one traps ^{40}K in the weaker lattice of $V_0 = 4E_{R\downarrow}$ (↓-fermions) and ^{6}Li in the stiffer lattice of $V_1 = 20E_{R\uparrow}$, then the Lieb lattice phase can be obtained for a scattering length of a_s (KLi) ≈ -80 nm. Such a strongly attractive scattering length

can be experimentally realized using the narrow Feshbach resonance for a ^{40}K-^{6}Li mixture by tuning the magnetic field at the milligauss accuracy [44]. The possible temperature range to achieve a Lieb lattice structure is determined by the bandwidth of the excess mobile fermions. For a scattering length of $a_s/a \sim -0.5$, the Lieb lattice phase is achievable as long as the temperature is lower than $J_{01} \sim 0.1E_R$. For lithium mixtures this translates to a temperature scale of ∼100 nK and for potassium-lithium mixtures the corresponding temperature is ∼20 nK.

One important process that can hinder experimental realization of the present scheme is the heating due to photon scattering in a deep optical lattice for ↑-fermions. It is known that the optical lattice depth is proportional to $\sim(\delta\omega)^{-1}$ and the photon scattering rate is proportional to $\sim(\delta\omega)^{-2}$, where $\delta\omega$ is the detuning of the laser frequency. For a far-detuned laser creating a shallow optical lattice for ↓-fermions, from Ref. [45] we took the heating rate, $\dot{T}_\downarrow \approx 10^{-4}E_R$/ms for ^{6}Li and $\approx 5.10^{-5}E_R$/ms for ^{40}K for a laser wavelength of 1064 nm. Then using the relation among the lattice depth, photon scattering rate, and detuning, one can find an estimate for the heating rate in the deeper lattices from the ratio, $\dot{T}_\uparrow/\dot{T}_\downarrow \approx (V_1/V_0)^2$. For lattice depths of $V_1 = 20E_R$ and $V_0 = 4E_R$ we find that $\dot{T}_\uparrow \sim 0.002E_R$/ms for ^{6}Li and $\dot{T}_\uparrow \approx 0.001E_R$/ms for ^{40}K. As the bandwidth of the Lieb lattice is of the order of $\sim 0.1E_R$, this restricts the duration of the experiments to ∼100 ms for both lithium and potassium mixtures. The limiting effect of radiative losses, in principle, could be eliminated by using alkaline-earth atoms, like ytterbium. Ytterbium does not allow for magnetic Feshbach resonances but can permit confinement-induced resonances in ultratight traps [46]. Yet another, so far relatively unexplored, option would be to use alkali–earth alkali mixtures like ytterbium-lithium [47]. Recently it has been proposed that due to hyperfine coupling between the electron spin and the nuclear magnetic moment, magnetic Feshbach resonance (width ∼2.8 mG) will occur between ground-state fermionic ytterbium and lithium atoms [48].

Next, we examine the effect of two-body and three-body inelastic loss processes. Due to the anticommutation relation between fermions of the same species (irrespective of the orbitals they occupy), the three-body loss from s-wave collisions vanishes. Then two-body collisions become the dominant loss process. To look into a particular example, we choose a ^{40}K-^{6}Li mixture, where two-body losses occur due to spin relaxation [49]. We define the two-body decay rate as $L = L_2 \int \mathcal{W}^s_{\mathbf{i},\downarrow}(\vec{r})\mathcal{W}^s_{\mathbf{i},\uparrow}(\vec{r})dr$, where $\mathcal{W}^M_{\mathbf{i},\sigma}(\vec{r})$ are Wannier functions at site i, for a species σ on a band M, and L_2 denotes the two-body loss rate. Then the particle loss rate is given by $N(t) = N(0)\exp[-Lt]$, and the corresponding lifetime is $\sim L^{-1} \sim 1$ s for $L_2 \sim 10^{-13}$ cm^3/s and a lattice constant of $a \sim 500$ nm. Also, for Feshbach resonances in ground-state alkali-earth alkali mixtures [48], such two-body loss processes will be absent.

We conclude this section by discussing briefly the effect of impurities which can appear in experimental realizations of CH1 structures. Such impurities can appear in the form of excess composites or missing composites in CH1 structures. These defects are reminiscent of the interstitial defects in solid-state crystals. The presence of such defects will create local regions with tunneling between p-p orbitals of strength $\sim J_p = J_1 + 2J_{11}$ or tunneling between s-s orbitals of strength $\sim J_0$. In the limit of dilute impurities, one can estimate the effective impurity strength as $g_{\rm imp} \sim n_{\rm imp}\max[J_p^2, J_0^2]/W^2$, where $n_{\rm imp}$ is the impurity density with $n_{\rm imp} \ll 1/2$ and W is the bandwidth of the clean lattice. From Eq. (7) we see that when $\Delta \sim 0$, the bandwidth is given by $W \sim J_{01}$, and when $\Delta \ll 0$, the bandwidth changes to $W \sim J_{01}^2/\Delta$. Now as long as $g_{\rm imp} \ll 1$, one can recover the clean limit of the dispersion relation with the density of states for the flat band showing a width of the order of $g_{\rm imp}$ [50]. Assuming an impurity concentration of $n_{\rm imp} = 0.05$, we find that $g_{\rm imp} \sim n_{\rm imp} = 0.05$ for $\Delta = 0$ and $g_{\rm imp} \sim 2n_{\rm imp} = 0.1$ for $\Delta \approx 2J_{01}$ for $a_s/a \sim -0.7$ for the parameters shown in Fig. 2. Thus we find that dilute impurities will have negligible effects on the properties of Lieb lattices.

VI. DYNAMICAL TOPOLOGICAL INSULATORS

The dynamical realization of a Lieb lattice opens up an alternative way to study the possibility of generating integer quantum Hall effects with cold-atom systems. One possible way to generate quantum Hall states such as QAH and QSH states in nontrivial lattices is by inducing effective spin-orbit coupling [51,52]. Such coupling can be achieved through optical means [53], by lattice shaking [54], or dynamically by including long-range interactions [56,57]. In our proposals we use the last of these methods and effective spin-orbit coupling is induced by the mean-field effect of the long-range interaction.

Models with long-range interactions are usually hard to implement in an experimentally realizable system, as the on-site interaction has to be of the same order of magnitude as the long-range part [58]. To investigate this possibility in our system we add an extra magnetic dipolar term (restricting its range to next-nearest neighbors) for the excess ↓-fermions,

$$\begin{aligned} H_{\rm full} &= H + H_{\rm dd}, \\ H_{\rm dd} &= U_{\rm dd}\sum_{\mathbf{i},\tau}\hat{n}_{x\tau\mathbf{i}}\hat{n}_{y\tau\mathbf{i}} + \frac{U_{\rm xy}}{2}\sum_{\langle\langle\mathbf{i},\mathbf{j}\rangle\rangle,\tau\neq\tau'}\hat{n}_{x\tau\mathbf{i}}\hat{n}_{y\tau'\mathbf{j}} \\ &\quad + \frac{U_{\rm xx}}{2}\sum_{\langle\langle\mathbf{i},\mathbf{j}\rangle\rangle,\tau}[\hat{n}_{x\tau\mathbf{i}}\hat{n}_{x\tau\mathbf{j}} + \hat{n}_{y\tau\mathbf{i}}\hat{n}_{y\tau\mathbf{j}}], \end{aligned} \tag{9}$$

where $U_{\rm dd}$ is an on-site dipolar interaction, U_{xy} is an interaction between particles in p_x and p_y orbitals at sites B and C, respectively, and U_{xx} is a next-nearest-neighbor interaction between particles in p_x and p_x orbitals (also between p_y and p_y orbitals) at sites B and C. $\langle\langle\mathbf{i},\mathbf{j}\rangle\rangle$ denotes next-nearest-neighbor p-orbital sites. We additionally introduce the dimensionless dipolar interaction strength $D = \mu_0\mu^2 m_\downarrow/2\hbar^2 a$, where μ is the magnetic dipole moment of the atoms and μ_0 is the vacuum permeability. The dipole-dipole interaction has the form $U_{\rm dd}(r) = D(1 - 3z^2/r^2)/r^3$, where r is the inte-particle distance. Effectively the fermions have a 2D nature so all the dipolar interaction terms are repulsive. For experimental realization, the suitable candidates are fermionic ^{161}Dy, which is experimentally available in a quantum degenerate state [59], and fermionic ^{167}Er [60]. Dy and Er could also be suitable due to the possibility of achieving lattices with laser wavelengths of ∼400 nm as discussed in Ref. [59]. This reduces the s-wave

scattering length needed to achieve the emergent Lieb lattice phase to $a_s \sim -100$ nm. Although, due to the presence of a zoo of Feshbach resonances in these atoms, one probably needs high tunability of the magnetic field. One can also use polar molecules provided that the short-range interaction is modified, for instance, using confinement-induced resonances.

Due to the strong attractive contact interaction $|U|$, the effect of dipolar terms on Δ is negligible. Moreover, we neglect the effective long-range repulsion between the composites, which can further stabilize the dynamical Lieb lattice phase. Then within the weak-coupling limit the mean-field parameters can be defined:

$$\begin{aligned}\langle \hat{p}^{\dagger}_{xBi}\hat{p}_{yCj}\rangle &= \langle \hat{p}^{\dagger}_{yBi}\hat{p}_{xCj}\rangle = i\chi_{\mathrm{QAH}},\\ \langle \hat{p}^{\dagger}_{xBi}\hat{p}_{yCj}\rangle &= -\langle \hat{p}^{\dagger}_{yBi}\hat{p}_{xCj}\rangle = i\chi_{\mathrm{QSH}},\\ \langle \hat{n}_{xBi}\rangle - \langle \hat{n}_{yCj}\rangle &= \langle \hat{n}_{xCi}\rangle - \langle \hat{n}_{yBj}\rangle = \chi_{\mathrm{SN}},\end{aligned} \tag{10}$$

where χ_{QAH} denotes the order parameter for the QAH state. QAH is characterized by a loop-current, broken time-reversal symmetry, and topologically protected chiral-edge states. The QSH-state order parameter χ_{QSH} can be thought of as two copies of QAH which, on the whole, conserve time-reversal symmetry [55]. This state contains helical edge states as shown in [61]. We see that the mean-field effect of the interaction effectively creates a spin-orbit coupling. The last order parameter χ_{SN} refers to the spin-nematic (SN) state. It breaks C_4 symmetry between the blue and the red sublattices and constitutes an anisotropic semimetal [57]. Near the QBCP, the mean-field energy is then given by

$$E_{\mathrm{mean}} = -\sum_{\mathbf{k}} E_{\mathbf{k}} + \left[U_{xy} + \frac{U_{\mathrm{dd}} - |\delta U_3|}{4}\right]\chi_{\mathrm{SN}}^2 + U_{xy}\chi^2, \tag{11}$$

where the dispersion relation is given by $E_{\mathbf{k}} = \sqrt{[(k_y^2 - k_x^2) - (U_{xy} + \frac{U_{\mathrm{dd}}-|\delta U_3|}{4})\chi_{\mathrm{SN}}]^2 + 4k_x^2k_y^2 + U_{xy}^2\chi^2}$, and the order parameter $\chi = \chi_{\mathrm{QAH}}$ or $\chi = \chi_{\mathrm{QSH}}$. Then we find various order parameters by minimizing the mean-field energy E_{mean}. We have calculated how these order parameters change with interaction strength $\alpha = a_s/a$ and dipolar strength D. The obtained phase diagram is presented in Fig. 3(d). We see that for a lower dipolar strength D one can stabilize quantum Hall states, whereas for a higher dipolar strength, the SN state minimizes the energy. This can be qualitatively explained by the fact that for weaker values of D, the repulsive dipolar on-site energy (U_{dd}) in Eq. (9) is compensated by the effective on-site attraction δU_3 in Eq. (6). Consequently, the mean-field physics is dominated by the long-range part of the dipolar terms, which results in stabilization of the QAH and QSH states. Even a low dipolar strength will make the system unstable towards the QAH and QSH states, but the gap in the bulk will be exponentially small. In that case, one needs very low temperatures to observe such phases. On the other hand, for a much higher dipolar strength, the repulsive on-site energy dominates the other interactions, which, in turn, stabilizes the SN phases. Within the mean-field ansatz, (10), both QAH and QSH have the same energy, although this degeneracy can be broken by including higher order exchange interactions [56]. The corresponding mean-field transition temperature to the QAH and QSH state is given by $T_c \sim (4J_{01}^2/\Delta)\exp[-J_{01}^2/2U_{xy}\Delta] \sim 0.01E_R$ for $D = 0.29$ and $\alpha = -0.7$. This dipolar strength can be reached in fermionic dysprosium with lattice constant of $a = 500$ nm and in fermionic erbium with a lattice constant of $a = 300$ nm.

VII. CONCLUSION

In conclusion, we have presented a theoretical proposal on how frustrated lattices can be created as an effect of self-assembly of cold atoms. We believe that our proposal opens up another fascinating route for experimental and theoretical studies of frustrated systems. The proposed scheme is very general and can be extended to other lattice structures even in three dimensions. Moreover, by varying the fermionic densities one can get different composite structures where different lattice geometries can be realized by the moving excess $\downarrow$-fermions. On the other hand, our proposal gives potential facilitation for the experimental realization of topological insulator. Namely, it does not involve additional optical components other than the ones needed for creating the parent lattice.

ACKNOWLEDGMENTS

We would like to thank Jakub Zakrzewski for simulating discussions and Michał Maik for providing valuable suggestion to improve the manuscript. We acknowledge the support by the EU STREP EQuaM, IP AQUTE and SIQS, ERC Grant QUAGATUA, AAII-Hubbard. O.D. also acknowledges support from National Science Centre Poland project DEC-2012/04/A/ST2/00088. A.P. is supported by the International PhD Project "Physics of future quantum-based information technologies", grant MPD/2009-3/4 from Foundation for Polish Science and by the University of Gdansk grant BW 538-5400-0981-12. A.P. also acknowledges hospitality from ICFO. Calculations were carried out at the Academic Computer Center in Gdansk.

APPENDIX A: DERIVATION OF J_{01} AND J_{11} IN THE MODIFIED HAMILTONIAN

Here we describe the procedure to calculate the terms in the modified Hubbard model in Eqs. (1), (2), and (3). The fermions are moving in the potential

$$\begin{aligned}V_{\sigma,\mathrm{latt}} = V_{\sigma,x}\sin^2(\pi x/a) + V_{\sigma,y}\sin^2(\pi y/a)\\ + V_{\sigma,z}\sin^2(\pi z/a),\end{aligned}$$

where $\sigma = \uparrow,\downarrow$ denotes the two species fermions and $V_{\sigma,x(y)(z)}$ are the corresponding lattice depths for σ-fermions along the x, y, and z directions, respectively. To create a 2D geometry, we choose $V_0 = V_{\downarrow,x} = V_{\downarrow,y}$, $V_1 = V_{\downarrow,z} = V_{\uparrow,x(y)(z)}$, and $V_1 \gg V_0$, which means that the $\downarrow$-fermions can effectively move in the x-y plane with the z motion frozen. The contact-interaction Hamiltonian is given by

$$H_{\mathrm{con}} = \frac{g}{2}\sum_{\sigma\neq\sigma'}\int \hat{\Psi}^{\dagger}_{\sigma}(\vec{r})\hat{\Psi}^{\dagger}_{\sigma'}(\vec{r})\hat{\Psi}_{\sigma'}(\vec{r})\hat{\Psi}_{\sigma}(\vec{r})d\vec{r}, \tag{A1}$$

where the field operators $\hat{\Psi}^{\dagger}_{\sigma}(\vec{r})$ and $\hat{\Psi}_{\sigma}(\vec{r})$ denote the creation and destruction operators at position $\vec{r}$ for fermionic species σ.

We also assume, for simplicity, that the mass of the two species is the same, $m_\uparrow = m_\downarrow = m$. The contact interaction is given by $g = 4\pi\hbar^2 a_s/m$. From that, we construct the Wannier functions $\mathcal{W}^M_{\mathbf{i},\sigma}(x,y,z) = \omega^{m_x}_{i_x,\sigma}(x)\omega^{m_y}_{i_y,\sigma}(y)\omega^{m_z}_{i_z,\sigma}(z)$ localized at site $\mathbf{i} = (i_x,i_y,i_z)$, which correspond to band $M = (m_x,m_y,m_z)$ [62]. Due to strong trapping along the z direction, we only take into account the lowest level in that direction. By expanding the field operators in the Wannier basis, we derive the parameters for the Hubbard model. In particular, the integrals used to calculate the s-p hopping term J_{01} and the correlated hopping term in the p band J_{11} are

$$\begin{aligned}\frac{J_{01}}{E_R} &= \frac{8\pi^2 a_s}{a}\int d\boldsymbol{r}\mathcal{W}^{100}_{\mathbf{i},\downarrow}(\boldsymbol{r})\left[\mathcal{W}^{000}_{\mathbf{i},\uparrow}(\boldsymbol{r})\right]^2\mathcal{W}^{000}_{\mathbf{j},\downarrow}(\boldsymbol{r}),\\ \frac{J_{11}}{E_R} &= \frac{8\pi^2 a_s}{a}\int d\boldsymbol{r}\mathcal{W}^{100}_{\mathbf{i},\downarrow}(\boldsymbol{r})\left[\mathcal{W}^{000}_{\mathbf{i},\uparrow}(\boldsymbol{r})\right]^2\mathcal{W}^{100}_{\mathbf{j},\downarrow}(\boldsymbol{r}),\end{aligned} \tag{A2}$$

where **ij** denote the nearest-neighboring sites along the x direction. As depicted in Figs. 1(b)and 1(c), the effective tunneling in the p band is given by $J_p = J_1 + 2J_{11}$. Subsequently, corresponding to the Hamiltonian in Eq. (2), we plot the magnitudes of the corresponding parameters in Fig. 5. We see that with increasing attraction, the effective hybridized tunneling J_{01} becomes comparable to the tunneling in the p band, denoted J_p. Additionally, we plot the energy cost Δ [as defined after Eq. (2)] as a function of the effective interaction a_s/a in Fig. 5. For small $|a_s|/a_s$, the energy cost Δ is positive. As one increases the attraction, Δ decreases, and for $a_s/a \lessapprox -0.56$, Δ becomes negative. Now the appearance of the CH1 state is favored when the s-p tunneling strength becomes of the same order of magnitude as the tunneling in the p band with $J_{01} \approx J_p = J_1 + J_{11}$ for $\Delta \lesssim 0$. From Fig. 5 we see that around $|\alpha| \sim 0.5$–0.6 both the tunnelings have the same order of magnitude, facilitating the checkerboard phase.

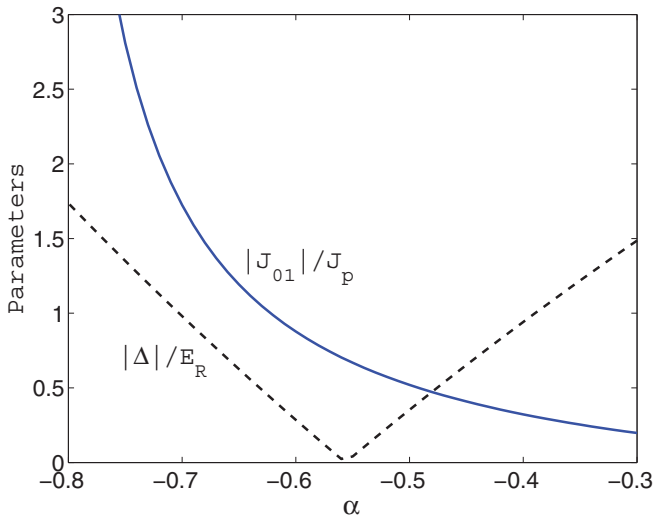

FIG. 5. (Color online) Important parameters in this paper: the energy cost $|\Delta|/E_R$ (dashed black line) and the relative strength of the s-p-band tunneling and the effective tunneling in the p band, $J_{01}/|J_p|$ [solid (blue) line], as a function of the effective interaction strength $\alpha = a_s/a$. We fix the $\downarrow$-fermion lattice depth $V_0 = 4E_R$ and the $\uparrow$-fermion lattice depth $V_1 = 30E_R$, for which we see from Fig. 2 that the CH1 state is stable. For low α, Δ is positive. As α becomes more negative, Δ decreases. For $\alpha \lessapprox -0.56$, Δ becomes negative and its absolute value increases. From the solid (blue) curve we also see that with an increase in $|\alpha|$, the effective p-band tunneling decreases and s-p tunneling increases, resulting in an increase in the ratio J_{01}/J_p. Around $\alpha \sim -0.6$ the contributions of all tunneling processes become of the same order of magnitude, facilitating the stability of the CH1 phase in the paper.

APPENDIX B: DERIVATION OF U_3 AND U_2 IN THE MODIFIED HAMILTONIAN

Next we describe the procedure for generating the effective interactions U_2 and U_3 in the modified Hamiltonian, Eq. (2). As described, one of the main parameters which controls the transition is the energy cost $\Delta = E_1 - |U_3| + |U_2|$. Thus the main quantity to consider is the difference $U_3 - U_2$. To do that we expand (A1) in terms of the Wannier functions at site **i**,

$$\begin{aligned}H_{\mathbf{i}} = &\sum_{MNPQ} f_{MNPQ}\hat{c}^\dagger_{M,\mathbf{i}}\hat{b}^\dagger_{N,,\mathbf{i}}\hat{b}_{P,,\mathbf{i}}\hat{c}_{Q,,\mathbf{i}}\\ &+\sum_M E^c_M\hat{c}^\dagger_{M,\mathbf{i}}\hat{c}_{M,\mathbf{i}} + \sum_M E^b_M\hat{b}^\dagger_{M,\mathbf{i}}\hat{b}_{M,\mathbf{i}},\end{aligned} \tag{B1}$$

where $MNPQ$ are the band indices and $\hat{c}^\dagger_{M,\mathbf{i}}$ and $\hat{c}_{M,\mathbf{i}}$ denote the creation and annihilation operators for $\downarrow$-fermions at site **i** and band M. Similarly, $\hat{b}^\dagger_{N,\mathbf{i}}$ and $\hat{b}_{N,\mathbf{i}}$ denote the creation and annihilation operators for $\uparrow$-fermions at site **i** and band N. E^c_M and E^b_M are the single-particle energies for $\downarrow$ and $\uparrow$-fermions, respectively, at band M. The effective strengths f_{NMPQ} are given in terms of the Wannier functions as

$$\frac{f_{MNPQ}}{E_R} = \frac{8\pi^2 a_s}{a}\int d\boldsymbol{r}\mathcal{W}^M_{\mathbf{i},\downarrow}(\boldsymbol{r})\mathcal{W}^N_{\mathbf{i},\uparrow}(\boldsymbol{r})\mathcal{W}^P_{\mathbf{i},\uparrow}(\boldsymbol{r})\mathcal{W}^Q_{\mathbf{i},\downarrow}(\boldsymbol{r}).$$

Now to determine U_2, first we assume that the particles occupy the lowest band. Then we calculate the effect of higher bands within the second-order perturbation theory by taking into account transitions to higher bands. Then the Hamiltonian is

$$\begin{aligned}H_2 &= -|f_{0000}|\hat{c}^\dagger_{0,\mathbf{i}}\hat{b}^\dagger_{0,\mathbf{i}}\hat{b}_{0,\mathbf{i}}\hat{c}_{0,\mathbf{i}} + \sum_M E^c_0\hat{c}^\dagger_{0,\mathbf{i}}\hat{c}_{0,\mathbf{i}}\\ &\quad + \sum_M E^b_M\hat{b}^\dagger_{0,\mathbf{i}}\hat{b}_{0,\mathbf{i}},\\ H_{2\text{pert}} &= \sum_{M>0} f_{M000}\hat{c}^\dagger_{M,\mathbf{i}}\hat{b}^\dagger_{0,\mathbf{i}}\hat{b}_{0,\mathbf{i}}\hat{c}_{0,\mathbf{i}}\\ &\quad + \sum_{M>0N>0} f_{MN00}\hat{c}^\dagger_{M,\mathbf{i}}\hat{b}^\dagger_{M,\mathbf{i}}\hat{b}_{0,\mathbf{i}}\hat{c}_{0,\mathbf{i}},\end{aligned} \tag{B2}$$

where in the diagonal term H_2, the first term is the interaction energy of the fermions in the lowest band, and the next two terms denote the single-particle energies of the lowest bands for the c- and b-fermions. In the perturbative Hamiltonian $H_{2\text{pert}}$, the first term denotes the transition of fermion species c ($=\downarrow$) to higher levels due to the interaction, whereas the last term denotes the process where both c-fermions ($=\downarrow$) and b-fermions ($=\uparrow$) are transferred to an excited state. Then for

perturbation theory to be valid, the first condition is

$$\left|\frac{f_{M000}}{\left(E_M^c - E_0^c\right) + |f_{0000}| - |f_{M00M}|}\right| \ll 1,$$
$$\left|\frac{f_{MN00}}{\left(E_M^c - E_0^c\right) + \left(E_N^b - E_0^b\right) + |f_{0000}| - |f_{MNNM}|}\right| \ll 1. \tag{B3}$$

To look into their properties, first we note that $|f_{MNNM}|, |f_{M00M}|, |f_{M000}|, |f_{MN00}| < |f_{0000}|$, as the interaction in the lowest band, has the strongest value. In addition, $(E_M^c - E_0^c) > 0$, $(E_N^b - E_0^b) > 0$ for band indices $M, N > 0$. So the denominators are always positive and we have numerically checked that the fractions are much less than unity. This situation is drastically different for repulsive interactions, where the denominator can indeed vanish, making the perturbation theory invalid. Then within second-order perturbation theory we can write the two-fermion interaction energy:

$$U_2 = -|f_{0000}| - \sum_{M>0} \frac{f_{M000}^2}{\left(E_M^a - E_0^a\right) + |f_{0000}| - |f_{M00M}|} - \sum_{MN>0} \frac{f_{MN00}^2}{\left(E_M^a - E_0^a\right) + \left(E_N^b - E_0^b\right) + |f_{0000}| - |f_{MNNM}|}. \tag{B4}$$

Similarly, one can write the Hamiltonian pertaining to the situation where there are two $\downarrow$ (c) particles, one at the s band and another at the p_x band, and one $\uparrow$ (b) fermion at the s band. The corresponding interaction energy U_3 is written in second-order perturbation as

$$\begin{aligned} U_3 = &-|f_{0000}| - |f_{1001}| - \sum_{M\neq[0,1]} \frac{f_{M000}^2}{\left(E_M^c - E_0^c\right) + |f_{0000}| - |f_{M00M}|} - \sum_{M\neq[0,1]} \frac{f_{M001}^2}{\left(E_M^c - E_1^c\right) + |f_{1001}| - |f_{M00M}|} \\ &- \sum_{M\neq[0,1]N>0} \frac{f_{MN00}^2}{\left(E_M^c - E_0^c\right) + \left(E_N^b - E_0^b\right) + |f_{0000}| + |f_{1001}| - |f_{1MM1}| - |f_{MNNM}|} \\ &- \sum_{M\neq[0,1]N>0} \frac{f_{MN01}^2}{\left(E_M^c - E_1^c\right) + \left(E_N^b - E_0^b\right) + |f_{0000}| + |f_{1001}| - |f_{0MM0}| - |f_{MNNM}|}, \end{aligned} \tag{B5}$$

where the band index $1 = (100)$ denotes the p_x band. The individual series in Eqs. (B4) and (B5) do not converge with respect to the summation over band indices M and N, and one needs to regularize the interaction at higher energies. But in this paper we are only interested in the difference in energy $U_3 - U_2$ which converges as one takes bands with higher energies. In our parameter regime $U_3 - U_2$ converges for band indices $M = 15$. Convergence of the differences between the energies is also discussed in Ref. [63] using the harmonic approximation for the lattice sites.

APPENDIX C: NUMERICAL METHODS

To search for an optimal configuration of composites we use the simulated annealing method. This technique takes random walks through the problem space at a successively lower temperature-like parameter. The probability of accepting a configuration is determined by the Boltzmann distribution, which allows getting out of the local minimum. We start our calculations from the phase-separated configuration, and the configuration for each next step is chosen by randomly changing the places of n_c composites, where $n_c \leqslant N_L/6$ for N_L is the size of the lattice. Parameters in the calculations obviously depend on the lattice size. For an 8×8 lattice we have used the following: the initial temperature-like control parameter is lowered over time by use of the cooling schedule $T(t+1) = T(t)/\mu_T$, where $\mu_T = 1.008$; it starts at $T(0) = 0.009$ and continues to $T(t) < 1.0e-6$. For each step we try $n_{\text{tries}} = 150$ configurations and for each temperature we perform $n_{\text{iters}} = 200$ iterations. The parameters for a 12×12 (16×16) lattice are $\mu_T = 1.002$ (1.001), $n_{\text{tries}} = 400$ (600), and $n_{\text{iters}} = 500$ (800) iterations. Initial and final temperatures are the same for every lattice size. Simulated annealing gives us an approximate solution that, with a high probability, is the global minimum. However, it may happen that the obtained configuration is a local minimum. Hence, to eliminate such solutions, we perform a *second check*: We group all the obtained configurations for different lattice depths and interaction strengths and we treat this set as a new problem space. The small size of this space allows us to individually compare the energies of every configuration.

APPENDIX D: EFFECT OF THE TUNNELING OF ↑-FERMIONS IN DEEPER LATTICES

In this section we study the effect of tunneling of ↑-fermions on the Lieb lattice phase. We are especially interested in the case with $\Delta < 0$. The corresponding tunneling Hamiltonian fore ↑ fermions is written as

$$H_{\uparrow t} = -J_\uparrow^1 \sum_{\langle \mathbf{ij}\rangle} \hat{s}_{\uparrow \mathbf{i}}^\dagger + J_\uparrow^2 \sum_{\langle \mathbf{ij}\rangle} \hat{s}_{\uparrow \mathbf{i}}^\dagger (\hat{n}_{\downarrow i} + \hat{n}_{\downarrow j}) \hat{s}_{\uparrow \mathbf{j}}, \tag{D1}$$

where $\hat{s}_{\mathbf{i}}^\dagger$ and $\hat{s}_{\mathbf{i}}$ are the creation and annihilation operators for ↑-fermions at the s band and $J_\uparrow^1$ is the corresponding tunneling amplitude. The interaction-induced tunneling of ↑-fermions at the s band is denoted $J_\uparrow^2$. When the band is filled for ↓-fermions, then approximately each neighbor of an ↑-fermion is filled by a ↓-fermion. Then the total tunneling is given by

$$J_\uparrow = J_\uparrow^1 + J_\uparrow^2.$$

In the case where $\Delta < 0$, but small, the Lieb lattice structure is definitely stable, provided $|J_{01}| \gg J_\uparrow$. This is the case in the strongly attractive limit, as even for $V_1 = 10E_R$ and $V_0 = 4E_R$, $|J_{01}|/J_\uparrow \sim 8$ with $a_s \sim -0.6$. In the case where $\Delta \ll 0$, each composite occupied site is also occupied by a $\downarrow$-fermion in the p orbital. Then the Lieb lattice structure is again stable, provided $J_{01}/\Delta \gg J_\uparrow/E_1$, which is also satisfied, as the energy gap of the p orbital (E_1) is much higher than Δ due to the attractive interaction. This condition can be proved trivially by looking into the second-order energy conserving processes which can delocalize the composite.

[1] P. W. Anderson, Science, New Series **177**, 393 (1972).
[2] G. M. Whitesides and B. Grzybowski, Science **295**, 2418 (2002).
[3] M. Lewenstein, A. Sanpera, and V. Ahufinger, *Ultracold Atoms in Optical Lattices: Simulating Quantum Many-Body Systems* (Oxford University Press, London, 2012).
[4] J. Struck *et al.*, Science **333**, 996 (2011).
[5] G.-B. Jo *et al.*, Phys. Rev. Lett. **108**, 045305 (2012).
[6] G. Wirth, M. Ölschläger, and A. Hemmerich, Nat. Phys. **7**, 147 (2011).
[7] L. Tarruell *et al.*, Nature **483**, 302 (2012).
[8] M. Aidelsburger *et al.*, Phys. Rev. Lett. **107**, 255301 (2011).
[9] P. Hauke *et al.*, Phys. Rev. Lett. **109**, 145301 (2012).
[10] K. Sun, W. V. Liu, A. Hemmerich, and S. Das Sarma, Nat. Phys. **8**, 67 (2012).
[11] T. Neupert, L. Santos, C. Chamon, and C. Mudry, Phys. Rev. Lett. **106**, 236804 (2011).
[12] N. Y. Yao *et al.*, Phys. Rev. Lett. **110**, 185302 (2013).
[13] M. Z. Hasan and C. L. Kane, Rev. Mod. Phys. **82**, 3045 (2010).
[14] X.-L. Qi and S.-C. Zhang, Rev. Mod. Phys. **83**, 1057 (2011).
[15] F. D. M. Haldane, Phys. Rev. Lett. **61**, 2015 (1988).
[16] C. Nayak *et al.*, Rev. Mod. Phys. **80**, 1083 (2008).
[17] J. K. Chin *et al.*, Nature **443**, 961 (2006).
[18] N. Strohmaier *et al.*, Phys. Rev. Lett. **99**, 220601 (2007).
[19] L. Hackermüller *et al.*, Science **327**, 1621 (2010).
[20] R. Micnas, J. Ranninger, and S. Robaszkiewicz, Rev. Mod. Phys. **62**, 113 (1990).
[21] A. Kuklov, N. Prokof'ev, and B. Svistunov, Phys. Rev. Lett. **92**, 030403 (2004).
[22] M. Lewenstein, L. Santos, M. A. Baranov, and H. Fehrmann, Phys. Rev. Lett. **92**, 050401 (2004).
[23] O. Dutta *et al.*, New J. Phys. **13**, 023019 (2011).
[24] T. Sowiński *et al.*, Phys. Rev. Lett. **108**, 115301 (2012).
[25] O. Dutta, T. Sowiński, and M. Lewenstein, Phys. Rev. A **87**, 023619 (2013).
[26] D.-S. Lühmann, O. Jürgensen, and K. Sengstock, New J. Phys. **14**, 033021 (2012).
[27] S. Will *et al.*, Nature **465**, 197 (2010).
[28] C. Chin, R. Grimm, P. Julienne, and E. Tiesinga, Rev. Mod. Phys. **82**, 1225 (2010).
[29] L. M. Falicov and J. C. Kimball, Phys. Rev. Lett. **22**, 997 (1969).
[30] T. Kennedy and E. H. Lieb, Physica A **138**, 320 (1986).
[31] S. Kirkpatrick, C. D. Gelatt, and M. P. Vecchi, Science **220**, 671 (1983).
[32] R. H. J. H. M. Otten, and L. P. P. P. van Ginneken, *The Annealing Algorithm* (Kluwer Academic, Boston, 1989).
[33] E. H. Lieb, Phys. Rev. Lett. **62**, 1201 (1989).
[34] A review of such systems can be found in Chapters 6 and 8 of Ref. [3].
[35] B. Schmidt *et al.*, Phys. Rev. Lett. **110**, 075302 (2013).
[36] B. Gadway *et al.*, Phys. Rev. Lett. **107**, 145306 (2011).
[37] J. Stenger, Phys. Rev. Lett. **82**, 4569 (1999).
[38] J. Steinhauer, R. Ozeri, N. Katz, and N. Davidson, Phys. Rev. Lett. **88**, 120407 (2002).
[39] E. Altman, E. Demler, and M. D. Lukin, Phys. Rev. A **70**, 013603 (2004).
[40] T. Bourdel *et al.*, Phys. Rev. Lett. **93**, 050401 (2004).
[41] M. Bartenstein *et al.*, Phys. Rev. Lett. **92**, 120401 (2004).
[42] C. H. Schunck *et al.*, Phys. Rev. A **71**, 045601 (2005).
[43] C. A. Regal and D. S. Jin, Phys. Rev. Lett. **90**, 230404 (2003).
[44] C. Kohstall *et al.*, Nature **485**, 615 (2012).
[45] D. C. McKay and B. DeMarco, Rep. Prog. Phys. **74**, 054401 (2011).
[46] B. Juliá-Díaz *et al.*, Nat. Commun. **4**, 2046 (2013).
[47] A. Khramov *et al.*, Phys. Rev. A **86**, 032705 (2012).
[48] D. A. Brue and J. M. Hutson, Phys. Rev. Lett. **108**, 043201 (2012).
[49] F. M. Spiegelhalder *et al.*, Phys. Rev. Lett. **103**, 223203 (2009).
[50] M. Vigh *et al.*, Phys. Rev. B **88**, 161413(R) (2013).
[51] R. Yu *et al.*, Science **329**, 61 (2010).
[52] C.-Z. Chang *et al.*, Science **340**, 167 (2013).
[53] J. Dalibard, F. Gerbier, G. Juzeliūnas, and P. Öhberg, Rev. Mod. Phys. **83**, 1523 (2011).
[54] J. Struck *et al.*, Phys. Rev. Lett. **108**, 225304 (2012).
[55] X.-L. Qi, Y.-S. Wu, and S.-C. Zhang, Phys. Rev. B **74**, 085308 (2006).
[56] S. Raghu, X.-L. Qi, C. Honerkamp, and S.-C. Zhang, Phys. Rev. Lett. **100**, 156401 (2008).
[57] K. Sun, H. Yao, E. Fradkin, and S. A. Kivelson, Phys. Rev. Lett. **103**, 046811 (2009).
[58] S. Uebelacker and C. Honerkamp, Phys. Rev. B **84**, 205122 (2011).
[59] M. Lu, N. Q. Burdick, and B. L. Lev, Phys. Rev. Lett. **108**, 215301 (2012).
[60] K. Aikawa *et al.*, Phys. Rev. Lett. **108**, 210401 (2012).
[61] C. Wu, B. A. Bernevig, and S.-C. Zhang, Phys. Rev. Lett. **96**, 106401 (2006).
[62] W. Kohn, Phys. Rev. **115**, 809 (1959).
[63] P. R. Johnson, E. Tiesinga, J. V. Porto, and C. J. Williams, New J. Phys. **11**, 093022 (2009).